Plurality of inherent states in equiatomic solid solutions

M. J. Demkowicz
Materials Science and Engineering, Texas A&M University, College Station, Texas 77843, USA
(Received 20 August 2016; revised manuscript received 14 February 2017; published 13 March 2017)

We show that single-crystal, equiatomic solid solutions of Lennard-Jones particles have a plurality of inherent states: mechanically stable configurations with identical lattice site occupancies, yet distinct potential-energy minima. External loading triggers transitions between inherent states via localized shear transformations. A plurality of inherent states and mechanically activated transitions between them make equiatomic solid solutions an unusual form of matter: one that is crystalline like single-component metals, yet exhibits localized shear transformations like metallic glasses.

DOI: 10.1103/PhysRevB.95.094108

I. INTRODUCTION

In classical linear elasticity theory of defect-free crystals, every applied load generates a unique field of atomic displacements [1]. This assumption requires that for any given distribution of atoms among lattice sites, there is just one mechanically stable, minimum energy configuration or "inherent state" [2,3]. Other inherent states may only be reached by nonelastic deformation through the motion of atoms to new lattice sites, e.g., due to the diffusion of vacancies [4] or propagation of dislocations [5].

We demonstrate that, contrary to the classical picture, in equiatomic solid solutions (ESSs) of misfitting particles, a single distribution of atoms among lattice sites possesses numerous inherent states: configurations with identical lattice site occupancies, yet distinct potential-energy minima. Mechanical loading triggers transitions between inherent states at loads well below those needed to nucleate dislocations, giving rise to localized shear transformations, in analogy to amorphous metals. Thus, equiatomic solid solutions are crystalline, like single-component metals, yet exhibit localized shear transformations, like metallic glasses. This finding has significant implications for the behavior of crystal defects in concentrated solid solutions, including properties such as the formation and interaction energies of dislocations or dislocation mobilities.

ESSs containing between two and five different metal elements (some of which are called "high entropy alloys" [6,7]) have garnered considerable attention on account of their unexpected thermodynamic stability [8] and attractive properties, such as high ductility and fracture toughness at cryogenic temperatures [9] or resistance to radiation-induced damage [10]. Our work does not focus on a specific alloy, by rather on the effect of atomic misfit on the mechanical stability of ESS crystal structure. We therefore investigate binary Lennard-Jones (LJ) mixtures: a common model system in condensed-matter physics [11–15]. We generate approximately equiatomic LJ solid solutions on a face-centered cubic (fcc) lattice by assigning one of two particle types to each lattice site at random with probability 0.5. Fcc crystals are the lowest energy states of single-component LJ structures [16,17]. We report all quantities in LJ units [18].

II. MODEL SYSTEM

The potential energy of a model containing N LJ particles may be written $V = \sum_{i=1}^{N-1} \sum_{j=i+1}^{N} \phi(r_{ij})$, where r_{ij} is the distance between particles i and j and the energy of a bond between them is

$$\phi(r_{ij}) = \begin{cases} 4\epsilon_{t_i t_j}\left[\left(\frac{\sigma_{t_i t_j}}{r_{ij}}\right)^{12} - \left(\frac{\sigma_{t_i t_j}}{r_{ij}}\right)^{6}\right] + \Delta\phi_{\text{cut}}, & r_{ij} \leqslant r_{\text{cut}} \\ 0, & r_{ij} > r_{\text{cut}} \end{cases}. \tag{1}$$

t_i denotes the type of particle i. $\epsilon_{t_i t_j}$ and $\sigma_{t_i t_j}$ are the characteristic bond energy and length, respectively, of the ij particle pair.

In a binary mixture, t_i takes on one of only two values: 1 or 2. In our models, $\epsilon_{t_i t_j} = 1$ for all pair types, $\sigma_{11} = 1$, $\sigma_{22} = \sigma$, and $\sigma_{12} = \sigma_{21} = \sqrt{\sigma_{11}\sigma_{22}} = \sqrt{\sigma}$. Here, σ is an adjustable parameter that tunes the misfit between particles of different types by altering their characteristic bond length. Without loss of generality, we take $\sigma \leqslant 1$. The bond energy $\phi(r_{ij})$ is zero for interparticle distances above $r_{\text{cut}} = 2.5\max(\sigma_{t_i t_j}) = 2.5$. The constant offset $\Delta\phi_{\text{cut}}$ ensures that there is no discontinuity in $\phi(r_{ij})$ at $r_{ij} = r_{\text{cut}}$. All of our models have periodic boundary conditions. We carry out molecular dynamics (MD) and molecular statics (MS) simulations [18] using LAMMPS [19] and visualize particle arrangements using AtomEye [20].

Single-crystal, fcc ESSs governed by Eq. (1) are mechanically stable for $\sigma \geqslant 0.84$. When $\sigma \leqslant 0.81$, the fcc crystal is unstable and collapses into an amorphous state. We reach these conclusions by scanning σ over [0.80,0.85] in increments of $\Delta\sigma = 0.01$. For each σ value, we create 50 independent realizations of a 500-particle fcc ESS, each with a different distribution of particle types across lattice sites. For each realization, we create 50 individual structures: one with all particles in ideal fcc positions and the rest with particles perturbed by displacements chosen at random from a uniform distribution on the surface of a sphere with radius 0.2. We relax each of the resulting 2500 structures to its nearest inherent state by minimizing its potential energy with respect to particle positions using the conjugate gradient method [21] while holding the simulation cell shape fixed. We then determine cumulative pair distribution functions (PDF) for each of the relaxed structures.

 ©2017 American Physical Society

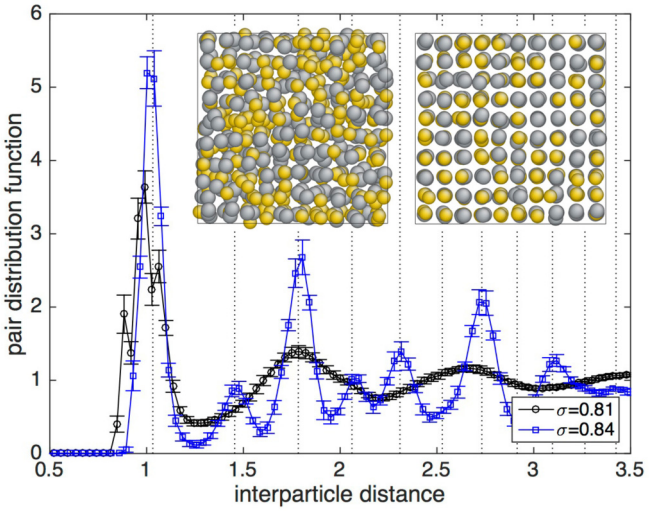

FIG. 1. Average PDFs for ESSs with $\sigma = 0.81$ and $\sigma = 0.84$. Vertical dotted lines indicate neighbor locations in an ideal fcc lattice. The insets are representative atomic structures for $\sigma = 0.81$ (left) and $\sigma = 0.84$ (right).

Figure 1 plots PDFs averaged over all 2500 relaxed structures for $\sigma = 0.81$ and $\sigma = 0.84$. It also shows representative particle structures for these two σ values. The $\sigma = 0.84$ PDF has peaks centered on the neighbor distances of an ideal fcc crystal out to distances of 3.5 (the maximum accessible in models of the size investigated), but broadened due to the misfit between the particles in the ESS. The particle structure for this σ value appears crystalline, albeit noticeably distorted from an ideal fcc state. By contrast, the PDF for $\sigma = 0.81$ resembles ones previously determined for amorphous particle packings [14,22,23]. It contains no evidence of crystalline ordering beyond the nearest-neighbor peak and the corresponding representative particle structure is evidently noncrystalline.

By analyzing differences between the average PDFs in Fig. 1 and the PDFs for each of the 2500 individual structures generated at a given σ value, we conclude that all of the individual PDFs exhibit the same qualitative features as their averages and therefore that all the individual fcc ESSs with $\sigma \geqslant 0.84$ remain crystalline while those with $\sigma \leqslant 0.81$ amorphize. The 2500 ESSs generated using $\sigma = 0.82$ and $\sigma = 0.83$ include both crystalline and amorphous structures. Binary LJ alloys are well known to form amorphous configurations for certain combinations of bond energies $\epsilon_{t_i t_j}$ and lengths $\sigma_{t_i t_j}$ [14,23]. Since the present investigation focuses on single crystal, fcc ESSs, we restrict the remainder of our calculations to $\sigma \geqslant 0.84$.

III. PLURALITY OF INHERENT STATES

To demonstrate that ESSs have a plurality of inherent states, we use MD to generate classical trajectories of duration $t_{\text{tot}} = 1000$ for models containing 4000 particles at temperatures of $T = 0.2$ (for comparison, the thermodynamic melting temperature of a single-component fcc LJ crystal with $r_{\text{cut}} = 2.5\sigma$ is $T_m \approx 0.66\epsilon$ [24]). We monitor mean-squared displacements to confirm that lattice site occupancies are always preserved: no particles migrate to new lattice sites in any of these simulations. We save snapshots of the atomic configuration at intervals of $\Delta t = 1$ and relax them to their nearest inherent states using the same method as described in Sec. II. In a single-component fcc crystal, all such relaxations yield identical structures: to high precision, the location $\vec{r}_i$ of each particle is the same in every structure and each structure has the same potential energy. Thus, single-component fcc crystals have just one inherent state for a given distribution of particles among lattice sites.

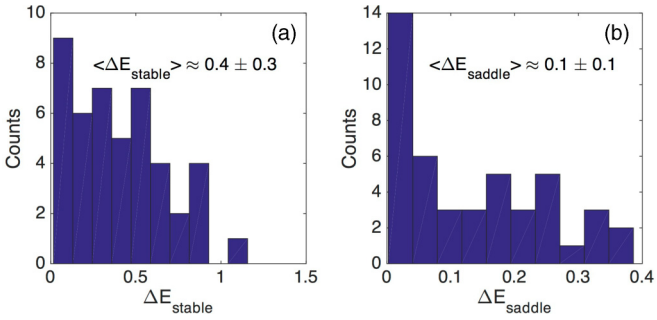

FIG. 2. Distributions of (a) energy differences, ΔE_{stable}, and (b) energy barriers, ΔE_{saddle}, between pairs of distinct inherent states in an ESS with $\sigma = 0.84$. The mean $\pm$ standard deviation is reported for each distribution.

By contrast, when we apply the procedure described above to ESSs, we find that the snapshots relax into multiple distinct inherent states. A pair of states is distinct if the minimum energy path connecting them passes through a saddle point in the potential-energy landscape. We use the climbing image nudged elastic band method (CINEB) [25,26] to find all of the distinct inherent states from among all 1000 snapshots. For $\sigma = 0.84$, our MD simulation yields $n_{is} = 10$ distinct inherent states. Figure 2 plots the distribution of energy differences, ΔE_{stable}, between these states (calculated going from the lower energy state to the higher energy state) as well as the distribution of energy barriers ΔE_{saddle} (calculated going from the higher energy state to the lower energy state). Both ΔE_{stable} and ΔE_{saddle} are on the order of a few tens of percent of a single LJ interparticle bond energy, $\epsilon_{t_i t_j} = 1$. We do not find any correlation between ΔE_{stable} and ΔE_{saddle}.

The number of inherent states in an ESS structure depends on the misfit σ as well as the degree of local compositional ordering. Repeating the analysis described above for $\sigma = 0.845$ and $\sigma = 0.85$, we find $n_{is} = 8$ and $n_{is} = 1$, respectively. Thus, the number of inherent states tends to decrease with decreasing misfit. To investigate the effect of local compositional ordering on n_{is}, we generate fcc LJ ESSs with the restriction that the average composition within the second-nearest-neighbor shell of every atom may not exceed a prespecified limit c_l. Unlike purely random distributions, such ESS structures do not contain regions that consist nearly entirely of type-1 or type-2 particles. We find that the number of distinct inherent states for $c_l = 0.6$ and $c_l = 0.55$ is $n_{is} = 12$ and $n_{is} = 6$, respectively. Thus, n_{is} appears to vary nonmonotonically with local ordering.

To understand the physical origin of the plurality of inherent states in ESSs, we investigate transitions between states in the previously described random ESS with $\sigma = 0.84$.

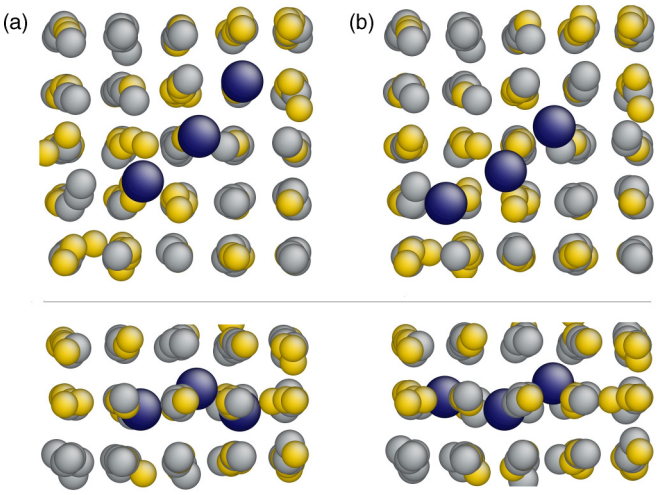

FIG. 3. Visualization of particles participating in a transition from the inherent state in column (a) to the one in column (b). The three participating particles are colored blue and lie along a ⟨110⟩ direction in a {100} plane, shown in plan view in the top row of images. The bottom row shows edge-on views of this {100} plane.

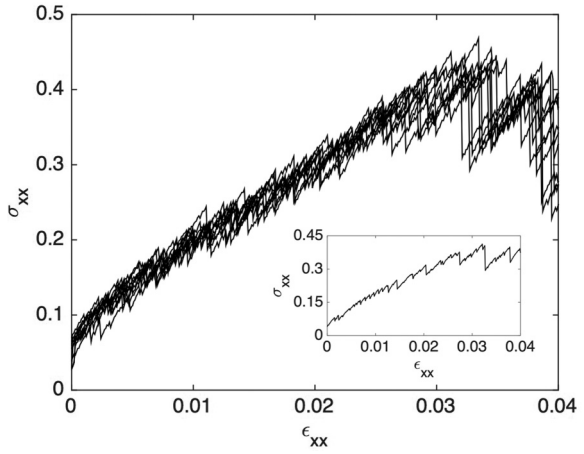

FIG. 4. Overlaid stress-strain curves, σ_{xx} vs ϵ_{xx}, for loading starting from each of the ten inherent states found in our random ESS model with $\sigma = 0.84$. The inset shows the stress-strain curve for loading starting from a single inherent state.

Forty-five distinct transitions may be enumerated for the ten inherent states in this model. We compute the particle displacements occurring in each transition and characterize the spatial extent of the associated structure change by finding the particles that undergo the largest displacements. We set the number of particles counted in each transition to be the participation number (PN), defined by Swayamjyoti *et al.* [15]. For each transition, we compute the radius of gyration R_g and composition c_{cluster} of the cluster of participating particles.

We find $\langle \text{PN} \rangle \approx 3.2 \pm 2.8$ and $\langle R_g \rangle \approx 2.2 \pm 1.8$ (reported as mean $\pm$ standard deviation), signifying that the changes in structure in each transition occur in a tightly limited volume. Moreover, $\langle c_{\text{cluster}} \rangle \approx 1.98 \pm 0.06$, i.e., clusters of participating particles are composed nearly exclusively of the smaller, type-2 particles. Thus, similar to disordered particle packings and amorphous solids [27,28], transitions between inherent states in ESSs preferentially occur in regions of greater free volume, where the motion of individual particles is less constrained by the surrounding elastic matrix. Figure 3 illustrates the change in particle arrangement that occurs during one of these transitions. The participating particles follow a string-like alignment along a ⟨l10⟩ direction in a {100} plane. They translate along a zig-zag trajectory as they pass between inherent states. Elements of this transition resemble the motion of a crowdion self-interstitial atom in fcc metals [29], with the key difference that the model shown in Fig. 3 does not contain any interstitial atoms.

IV. MECHANICALLY ACTIVATED TRANSITIONS BETWEEN INHERENT STATES

In an MD simulation, transitions between inherent states are thermally activated. Certain transitions may also be activated without thermal agitation by externally applied mechanical loads. We use MS simulations to investigate whether transitions between inherent states may be activated mechanically in our $\sigma = 0.84$, random ESS model. We begin by relaxing the ten inherent states generated via MD with respect to both atomic positions and simulation cell volume. This step is needed to relax the thermal expansion acquired during the MD simulation that was used to generate these structures.

Next, starting from one of these relaxed structures, we repeatedly apply small, volume-conserving increments of plane strain to the simulation cell until a desired level of deformation is reached [30]. Each strain increment holds the dimensions in the z direction fixed, extends the simulation cell along the x direction by a strain of 10^{-4}, and compresses the cell in the y direction by the amount required to maintain constant volume. No off-diagonal strains are applied. If re-expressed in a coordinate system rotated by 45° about the z axis, these strain increments are seen to be a nearly pure shear [31]. After each strain increment, we minimize the model energy with respect to particle positions while holding the simulation cell shape fixed, giving a mechanical equilibrium state at nonzero external load. We calculate the virial stresses borne by the simulation cell in these relaxed states.

Figure 4 plots normal stress in the x direction, σ_{xx}, against the corresponding normal strain ϵ_{xx} for monotonic loading starting from of each of the ten inherent states found in the random ESS with $\sigma = 0.84$. The general trend exhibited by these curves is of stress increasing approximately linearly with strain for strains below ~0.03 followed by a transition to plastic flow at higher strains. Closer inspection of individual stress-strain curves reveals that none of them possesses a strictly elastic portion, where stresses vary reversibly with strains. Rather, each exhibits irreversible stress drops, similar to those seen in simulations of displacement-controlled loading of amorphous solids [30,32].

These stress drops occur at all—even the lowest—levels of stress. Each one signals a mechanically activated transition between distinct inherent states. Because these transitions are localized, as shown in Fig. 3, and because they couple to external shear loads, they are in fact localized shear transformations (LSTs), in complete analogy to LSTs in amorphous solids [33,34] (also known as shear transformation zones or "STZs"

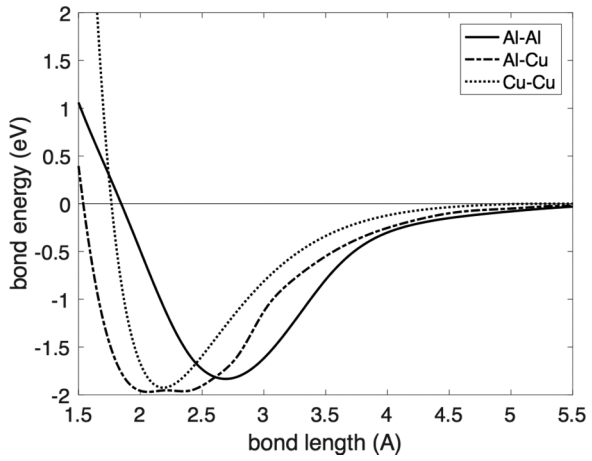

FIG. 5. Plots of energy vs bond length for Al-Al, Al-Cu, and Cu-Cu dimers.

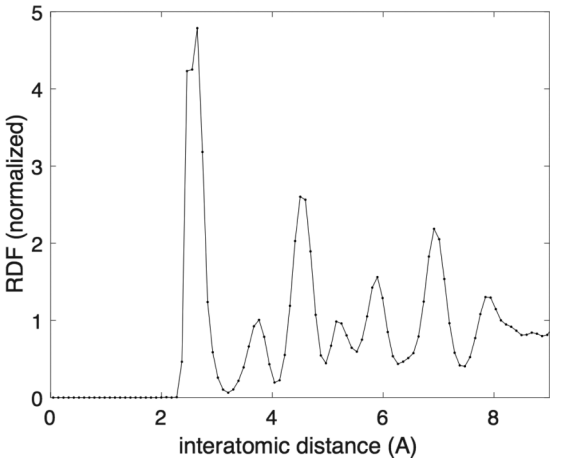

FIG. 6. RDF for an Al-Cu ESS, computed by averaging 2500 distinct models.

[35,36]). The high frequency of these transitions suggests that there may be many more distinct inherent states in this model than the ten identified in the previously described MD simulations.

V. MULTIPLICITY OF INHERENT STATES IN A CU-AL ESS

To verify that the plurality of inherent states identified in the foregoing sections is not an artifact of the very special form of the LJ potential, we investigate the Al-Cu system and show that it also exhibits a plurality of inherent states. We use the angular-dependent potential (ADP) for Al-Cu by Apostol and Mishin [37]. The ADP is not a pure pair potential. Similar to embedded atom method (EAM) potentials [38], the ADP possesses both pairwise and embedding energy terms. Moreover, it also includes several angle-dependent energy terms. Thus, the behavior of a LJ model cannot be expected to map directly onto that of an ADP model.

Figure 5 plots energy vs bond length for Al-Al, Al-Cu, and Cu-Cu dimers computed using this potential while Table I lists the equilibrium bond energies and bond lengths for all three dimer types. Based on these data, the ratio of nearest-neighbor distances for Cu and Al is 0.81. In view of our LJ simulations, this high degree of misfit makes the Al-Cu system a likely candidate to exhibit a multiplicity of inherent states. Figure 5 also shows that the Al-Cu dimer has two distinct minima. The energies of these minima are so close and the barrier between them is so small that it may be more appropriate to think of them as bounding a range of Al-Cu bond lengths with nearly constant bond energy.

TABLE I. Equilibrium bond energies and bond lengths for Al-Al, Al-Cu, and Cu-Cu dimers.

Dimer type	Index of equilibrium point	Bond energy (eV)	Bond length (Å)
Al-Al	1	−1.83	2.69
Al-Cu	1	−1.97	2.06
	2	−1.96	2.34
Cu-Cu	1	−1.92	2.19

Following the same approach as was used with the LJ models, we create a RDF for an Al-Cu ESS averaged over different Al and Cu distributions across lattice sites. This RDF, shown in Fig. 6, is consistent with a fcc crystal structure. None of the 2500 models used to generate this RDF show any evidence of amorphization.

As with the LJ models, we generate a series of 1000 atomic structures of an Al-Cu ESS by running an MD trajectory of a 4000-atom model and taking "snapshots" of the structure every 1000 time steps. This simulation is run at a temperature of 400 K, which corresponds to a homologous temperature of ∼0.3 in Cu and ∼0.43 in Al. By monitoring mean-square displacements, we confirm that there is no atom diffusion between different lattice sites during the simulation. Using the CINEB method [25,26], we examine the first 256 of the 1000 recorded structures and find that 32 of them are distinct inherent states. Each pair of these states is separated by an energy barrier, ΔE_{saddle}. Figure 7 plots distributions of the energy differences, ΔE_{stable}, between all pairs of these states (calculated going from the lower energy state to the higher energy state) as well as the distribution of ΔE_{saddle} (calculated going from the higher energy state to the lower energy state).

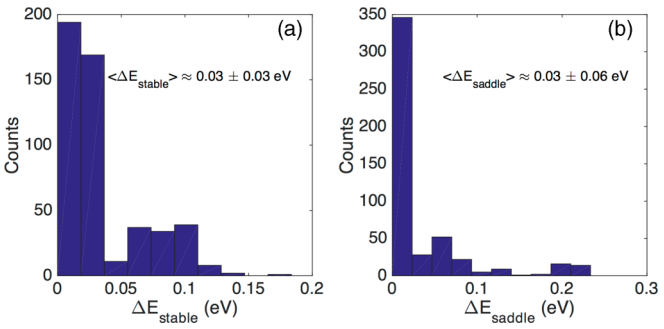

FIG. 7. Distributions of (a) energy differences, ΔE_{stable}, and (b) energy barriers, ΔE_{saddle}, between pairs of distinct inherent states in an Al-Cu ESS with. The mean ± standard deviation is reported for each distribution.

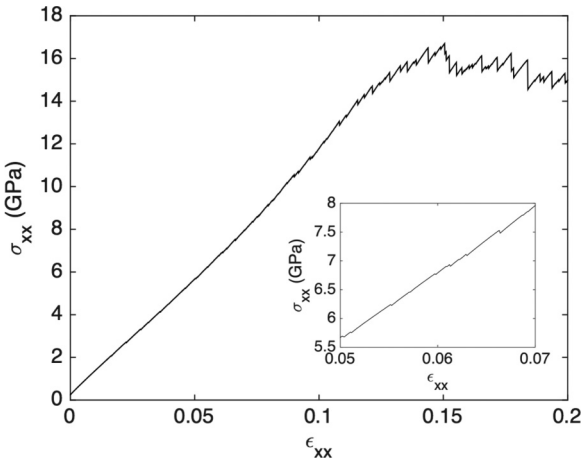

FIG. 8. Stress-strain curve for an Al-Cu ESS loaded under volume-conserving pure shear. The inset shows a portion of the stress-strain curve at approximately half the stress needed to initiate plastic flow.

These results predict that a plurality of inherent states may be expected in equiatomic solid solutions composed of Al and Cu.

The mean interatomic distance in our models is ∼2.6 Å. Meanwhile, the total atomic displacement distance involved in transitions between inherent states is ∼0.05 Å on average and never greater than ∼0.3 Å. These displacements are not large enough to bring the Al-Cu bond length within range of the bond energy minimum around 2 Å shown in Fig. 5. We therefore conclude that the shape of the Al-Cu dimer energy curve is not the cause of the observed plurality of inherent states in ADP Al-Cu. The small energy differences between inherent states in Al-Cu are due to the small atomic displacements that separate them.

Finally, we also conducted a simulation of mechanical shear loading of the Al-Cu ESS. The resulting stress-strain curve is shown in Fig. 8. It shows stress increasing approximately linearly with strain for strains below ∼0.12 followed by a transition to plastic flow at higher strains. This stress-strain curve does not possess a strictly elastic portion, where stresses vary reversibly with strains. Rather, even well before the onset of plastic flow, it exhibits irreversible stress drops, such as those illustrated in the inset of Fig. 8. These stress drops are due to localized shear transformations (LSTs), similar to those discussed in Sec. IV. The magnitude of the stress drops is not as large as for those found in a random LJ ESS with $\sigma = 0.84$. Further investigation is needed to determine what aspects of the interatomic interaction govern the magnitude of the stress drops associated with LSTs.

VI. DISCUSSION

A plurality of inherent states and the existence of mechanically activated transitions between them make ESSs an unusual form of matter: one that is crystalline like single-component metals, yet exhibits LSTs like metallic glasses. The presence of long-range, crystalline ordering means that ESSs may contain conventional crystal defects, such as dislocations. However, due to stress relaxation by LSTs, the elastic fields generated by these defects are not the same as those found in single-component crystals. In particular, LSTs are likely to reduce elastic strain energies of individual crystal defects as well as elastic interaction energies between pairs of defects, potentially altering defect-governed phenomena in ESSs such as strain hardening, radiation response, or epitaxial growth. They may also help to explain unique behaviors of ESSs. For example, the exceptionally strong dependence of ESS mechanical properties on temperature may be the outcome of temperature-dependent screening of dislocations from external stresses by LSTs [9,39–41].

Similarly, crystallinity leads to major differences between defect behavior in ESSs and metallic glasses. For example, although the classical Volterra cutting-and-welding operations for creating dislocations [5,42] may be carried out in any solid (including an amorphous one), the lack of long-range, crystalline ordering in amorphous solids means that the resulting elastic fields are not associated with a topologically conserved Burgers vector. Indeed, LSTs easily relax dislocationlike stress fields introduced into an amorphous solid *via* Volterra operations [43]. In ESSs, however, dislocations do have a topologically conserved Burgers vector. Thus, even though LSTs may relax a dislocation's stress fields to some degree, they cannot remove it entirely, unlike in a metallic glass.

Models such as the binary Lennard-Jones potential are not a substitute for the construction of chemically accurate simulations of real ESSs. However, they do give insights into qualitative physical behaviors, such as the emergence of a plurality of inherent states at sufficiently high atomic misfit. Based on these insights, we expect that binary ESSs with large atomic misfit, such as Cu-Al [44], are more likely to exhibit a plurality of inherent states than ones with smaller misfit, such as Cu-Ni [45]. Our simulations also suggest that local atomic ordering influences the density of inherent states. Exhaustive enumerations of the number of inherent states in specific structures using specialized methods such as the activation-relaxation technique (ART) [46–48] may help to assess such trends more quantitatively.

Additional simulations will also be required to devise strategies for the experimental detection of multiple inherent states in ESSs. One avenue might be to determine whether mechanically induced transitions between these states (i.e., LSTs) give rise to an internal friction peak that may be detected using ultrasonic methods [49–51]. By comparing internal friction peaks measured experimentally to ones obtained from atomistic simulations, it may be possible to confirm the presence of LSTs in ESSs. Another approach may involve measuring thermal transport. Similar to rattling modes in ordered crystals, LSTs in ESSs may increase phonon scattering and thereby exert a measurable influence on lattice thermal conductivity [52,53]. Finally, a plurality of inherent states may give rise to excess entropy over and above that arising from configurational entropy in ESSs [8]: a property that may be measured through a variety of calorimetric and scattering methods [54].

ACKNOWLEDGMENT

M.J.D. acknowledges stimulating discussions with G. M. Pharr, T. Cagin, and A. Needleman.

[1] A. E. H. Love, *A Treatise on the Mathematical Theory of Elasticity*, 4th ed. (Dover, New York, 1944).
[2] F. H. Stillinger and T. A. Weber, Science **225**, 983 (1984).
[3] F. H. Stillinger and T. A. Weber, Phys. Rev. A **28**, 2408 (1983).
[4] P. G. Shewmon, *Diffusion in Solids*, 2nd ed. (Minerals, Metals & Materials Society, Warrendale, PA, 1989).
[5] J. P. Hirth and J. Lothe, *Theory of Dislocations*, 2nd ed. (Wiley, New York, 1982).
[6] B. Cantor, I. T. H. Chang, P. Knight, and A. J. B. Vincent, Mater. Sci. Eng. A **375-377**, 213 (2004).
[7] J. W. Yeh, S. K. Chen, S. J. Lin, J. Y. Gan, T. S. Chin, T. T. Shun, C. H. Tsau, and S. Y. Chang, Adv. Eng. Mater. **6**, 299 (2004).
[8] Y. Zhang, T. T. Zuo, Z. Tang, M. C. Gao, K. A. Dahmen, P. K. Liaw, and Z. P. Lu, Prog. Mater. Sci. **61**, 1 (2014).
[9] B. Gludovatz, A. Hohenwarter, D. Catoor, E. H. Chang, E. P. George, and R. O. Ritchie, Science **345**, 1153 (2014).
[10] T. Egami, M. Ojha, O. Khorgolkhuu, D. M. Nicholson, and G. M. Stocks, JOM **67**, 2345 (2015).
[11] T. F. Middleton, J. Hernandez-Rojas, P. N. Mortenson, and D. J. Wales, Phys. Rev. B **64**, 184201 (2001).
[12] F. Sciortino, W. Kob, and P. Tartaglia, Phys. Rev. Lett. **83**, 3214 (1999).
[13] R. Goetz and R. Lipowsky, J. Chem. Phys. **108**, 7397 (1998).
[14] W. Kob and H. C. Andersen, Phys. Rev. E **51**, 4626 (1995).
[15] S. Swayamjyoti, J. F. Loffler, and P. M. Derlet, Phys. Rev. B **89**, 224201 (2014).
[16] Y. Choi, T. Ree, and F. H. Ree, J. Chem. Phys. **99**, 9917 (1993).
[17] L. C. Flatley and F. Theil, Arch. Ration. Mech. Anal. **218**, 363 (2015).
[18] M. P. Allen and D. J. Tildesley, *Computer Simulation of Liquids* (Oxford University Press, Oxford, 1987).
[19] S. Plimpton, J. Comput. Phys. **117**, 1 (1995).
[20] J. Li, Model. Simul. Mater. Sci. Eng. **11**, 173 (2003).
[21] D. P. Bertsekas, *Nonlinear Programming*, 2nd ed. (Athena Scientific, Cambridge, MA, 1999).
[22] J. D. Bernal, Proc. R. Soc. London, Ser. A **280**, 299 (1964).
[23] G. Wahnstrom, Phys. Rev. A **44**, 3752 (1991).
[24] J. R. Morris and X. Y. Song, J. Chem. Phys. **116**, 9352 (2002).
[25] G. Henkelman, B. P. Uberuaga, and H. Jonsson, J. Chem. Phys. **113**, 9901 (2000).
[26] G. Henkelman and H. Jonsson, J. Chem. Phys. **113**, 9978 (2000).
[27] F. Spaepen, Acta Metall. **25**, 407 (1977).
[28] P. Schall, D. A. Weitz, and F. Spaepen, Science **318**, 1895 (2007).
[29] P. Ehrhart, in *Atomic Defects in Metals*, edited by H. Ullmaier (Springer-Verlag, Berlin, 1991).
[30] M. J. Demkowicz and A. S. Argon, Phys. Rev. B **72**, 245206 (2005).
[31] W. S. Slaughter, *The Linearized Theory of Elasticity* (Birkhäuser, Boston, 2002).
[32] C. E. Maloney and A. Lemaitre, Phys. Rev. E **74**, 016118 (2006).
[33] A. S. Argon, Acta Metall. **27**, 47 (1979).
[34] A. S. Argon and H. Y. Kuo, Mater. Sci. Eng. **39**, 101 (1979).
[35] M. L. Falk and J. S. Langer, Phys. Rev. E **57**, 7192 (1998).
[36] J. S. Langer, Phys. Rev. E **70**, 041502 (2004).
[37] F. Apostol and Y. Mishin, Phys. Rev. B **83**, 054116 (2011).
[38] M. S. Daw and M. I. Baskes, Phys. Rev. B **29**, 6443 (1984).
[39] Z. Wu, H. Bei, G. M. Pharr, and E. P. George, Acta Mater. **81**, 428 (2014).
[40] F. Otto, A. Dlouhy, C. Somsen, H. Bei, G. Eggeler, and E. P. George, Acta Mater. **61**, 5743 (2013).
[41] A. Gali and E. P. George, Intermetallics **39**, 74 (2013).
[42] V. Volterra, Ann. Sci. ENS **24**, 401 (1907).
[43] P. J. Steinhardt and P. Chaudhari, Philos. Mag. A **44**, 1375 (1981).
[44] Z. S. Basinski, R. A. Foxall, and R. Pascual, Scr. Metall. **6**, 807 (1972).
[45] M. Z. Butt, F. Aziz, and D. Ali, J. Alloy. Compd. **498**, 102 (2010).
[46] G. T. Barkema and N. Mousseau, Phys. Rev. Lett. **77**, 4358 (1996).
[47] N. Mousseau and G. T. Barkema, Phys. Rev. E **57**, 2419 (1998).
[48] R. A. Olsen, G. J. Kroes, G. Henkelman, A. Arnaldsson, and H. Jonsson, J. Chem. Phys. **121**, 9776 (2004).
[49] H. Wagner, D. Bedorf, S. Kuchemann, M. Schwabe, B. Zhang, W. Arnold, and K. Samwer, Nat. Mater. **10**, 439 (2011).
[50] M. Grewer, J. Markmann, R. Karos, W. Arnold, and R. Birringer, Acta Mater. **59**, 1523 (2011).
[51] A. Caron and W. Arnold, Acta Mater. **57**, 4353 (2009).
[52] W. Schweika, R. P. Hermann, M. Prager, J. Persson, and V. Keppens, Phys. Rev. Lett. **99**, 125501 (2007).
[53] D. J. Voneshen *et al.*, Nat. Mater. **12**, 1028 (2013).
[54] B. Fultz, Prog. Mater. Sci. **55**, 247 (2010).